Applied Catalysis B: Environmental 164 (2015) 92–99

Contents lists available at ScienceDirect

Applied Catalysis B: Environmental

journal homepage: www.elsevier.com/locate/apcatb

Manganese oxide octahedral molecular sieve (OMS-2) as an effective catalyst for degradation of organic dyes in aqueous solutions in the presence of peroxymonosulfate

Shilu Luo[a], Lian Duan[a], Binzhe Sun[a], Mingyu Wei[a], Xiaoxia Li[b], Aihua Xu[a,*]

[a] School of Environmental Engineering, Wuhan Textile University, Wuhan 430073, China
[b] School of Chemistry and Chemical Engineering, Wuhan Textile University, Wuhan 430073, China

ARTICLE INFO

Article history:
Received 11 July 2014
Received in revised form 5 September 2014
Accepted 6 September 2014
Available online 16 September 2014

Keywords:
OMS-2
Peroxymonosulfate
Acid Orange 7
Degradation

ABSTRACT

Cryptomelane type manganese oxide OMS-2 was prepared and tested in heterogeneous activation of peroxymonosulfate (PMS) for Acid Orange 7 (AO7) degradation in aqueous solutions. X-ray diffraction, scanning electron microscopy, N_2 adsorption/desorption isotherms, Fourier transform infrared spectroscopy, X-ray photoelectron spectroscopy (XPS), and electron spin resonance spectroscopy (ESR) were used to characterize the properties of the material. The effect of several parameters on its catalytic activity was also investigated. It was found that the catalyst was very active for AO7 and other organic dyes degradation, and presented a long-term stability during multiple runs. Results from XPS and ESR suggested that the highly catalytic efficiency possible involved the activation of PMS to sulfate radicals meditated by the redox pair of Mn(IV)/Mn(III) in OMS-2. Based on intermediate detections, the degradation pathway of AO7 in the OMS-2/PMS system was proposed.

1. Introduction

Efficient removal of organic contaminants is one of the major targeted objectives of water treatment and wastewater reclamation unit operators [1]. The advanced oxidation processes using reactive radicals are recognized as effective ways for degradation of organic pollutants dissolved in water [2–5]. In the past decades, sulfate radical based advanced oxidation technologies have become a hotspot due to its high oxidizing ability [6]. The radicals can be generated by activation of persulfate or peroxymonosulfate (PMS) by UV, heat and catalysts [7–9]. However, UV activation and thermal activation both need added energy, and transition metal ions catalysts such as Co(II), Cu(II), Mn(II), Ni(II) and Ce(III) are toxic and difficult to recycle. In recent years, the heterogeneous activation of PMS to degrade contaminants has become a more focused area [10–15]. For example, Chen et al. prepared nano-Co_3O_4 by precipitation method and investigated the performance of Co_3O_4/PMS system using Acid Orange 7 (AO7) as a model compound [16]. Zhang et al. found that cobalt oxide deposited on MgO exhibited very good and stable performance for the degradation of methylene blue dye with PMS [17]. Ji et al. reported a fast degradation of phenol by using CuO particles to activate PMS at pH 4.0 [18]. They also found that Fe_2O_3/PMS system exhibited high activity and stability in decolorization of Rhodamine B [19], and the porous structure and the great surface area can enhance the catalytic activity. More recently, $CuFe_2O_4$ magnetic nanoparticles have been suggested as efficient heterogeneous catalysts for PMS activation [20–22].

Besides cobalt, iron and copper oxides, other heterogeneous transition metal catalysts like manganese oxides have been widely investigated by Wang's group [23–28]. They studied several α-MnO_2 catalysts for heterogeneous activation of PMS to generate sulfate radicals for phenol degradation and found that MnO_2 exhibited varying activities depending on structure and morphology [23,26]. They also conducted a study on the heterogeneous catalytic degradation of phenol in aqueous solution on a series of manganese oxides [25]. The work showed that Mn_2O_3 is the best catalyst, with the sequence of catalytic activity as $Mn_2O_3 > MnO > Mn_3O_4 > MnO_2$, which was correlated with oxidation state and oxygen mobility on the catalysts.

Cryptomelane (OMS-2) is a form of manganese dioxide having a tunnel size of 0.46 nm × 0.46 nm, which is constructed from edge-shared double [MnO_6] octahedral chains [29]. The material exhibits salient features like mixed-valence (2+, 3+, and 4+) of Mn, a hydrophobic nature, porous structure, easy release of lattice oxygen, and acidic sites [30], and has been extensively studied in the area of catalysis, separations, ion exchange, and various

* Corresponding author. Tel.: +86 27 59367334; fax: +86 27 59367334.
E-mail address: xahspinel@sina.com (A. Xu).

http://dx.doi.org/10.1016/j.apcatb.2014.09.008
0926-3373/

applications related to energy and environmental fields [31–33]. Because the presence of mixed-valence manganese species in OMS-2, we anticipated the sieve as a powerful candidate for the catalytic activation of PMS. Therefore, OMS-2 was prepared by a simple reflux method and used as catalysts to generate reactive radical. The present work is aimed at investigating the effectiveness and feasibility of such a system in treatment of organic dyes. Complete characterization techniques were also employed to establish potential relationships between the properties (structure, morphology, porosity, and valence) and catalytic performance for the reaction. To the best of our knowledge, this is the first try to use OMS-2 as a catalyst for the degradation of dyes with PMS as the oxidant.

2. Materials and methods

2.1. Preparation of OMS-2 catalyst

OMS-2 was synthesized by a reflux method similar to that reported on the literature [33]. Briefiy, 60 mmol manganese sulfate hydrate ($MnSO_4$) was placed in 30 mL double deionized water (DDW) with 3 mL of nitric acid. A second solution was prepared by dissolving 38 mmol $KMnO_4$ in 100 DDW. This latter solution was subsequently added dropwise into the $MnSO_4$ solution under vigorous stirring to form a dark brown precipitate at 110 °C. The resultant slurry was heated overnight at the reflux temperature, washed with DDW, and finally dried at 120 °C for 12 h to obtain OMS-2. Another OMS-2 sample was also prepared fully in accordance with the processes in the literature [33], during which the solutions of $KMnO_4$ and $MnSO_4$ were first mixed at room temperature, then 3 mL of nitric acid was added. A dark brown slurry formed which was refluxed for 24 h at a temperature of 110 °C, then filtered, washed and finally dried at 120 °C overnight. This sample was referred as OMS-2 (2). For a comparison, a mesoporous MnO_2 sample was prepared by reduction of $KMnO_4$ with maleic acid [23].

2.2. Characterization

X-ray powder diffraction (XRD) pattern was obtained on a Bruker D8 powder X-ray Diffractometer with Cu $K\alpha$ radiation ($\lambda = 0.15406$ nm). The beam voltage and current used were 40 kV and 40 mA, respectively. Fourier transform infrared (FT-IR) spectra were recorded on a Bruker Vector 22 spectrometer. The sample was mixed with solid KBr, then ground into powder and dried before pressed into a KBr wafer. The surface morphology was characterized on a Hitachi S-4800 scanning electron microscope (SEM) instrument (Hitachi Ltd., Japan).

The determination of pore size distribution, BET surface area, and pore volume was carried out with a Quantachrome Autosorb-1 at −196 °C. The samples were first degassed at 200 °C for 6 h. The surface area of the samples was obtained using the N_2 adsorption isotherm with the Brunauer–Emmett–Teller equation. The average pore diameter was calculated with the Barrett–Joyner–Halenda desorption isotherm.

The chemical oxidation states of Mn species in OMS-2 were investigated by X-ray photoelectron spectra (XPS) on a VG Multilab 2000 spectrometer (Thermo Electron Corporation) with AlKa radiation as the exciting source (300 W). Charging effects were corrected by adjusting the binding energy of C 1s to 284.6 eV.

Electron spin resonance (ESR) spectra were recorded at room temperature using a Bruker ESR A-300 spectrometer with the following parameters: center field 3450 G, sweep width 1500 G, microwave frequency 9.86 G, modulation frequency 100 kHz, microwave power 1 mW.

2.3. Catalytic degradation experiment

Degradation reactions were performed in a 100 mL open flask at ambient temperature and under normal laboratory light. The flask was putted in a shaker at a stirring speed of 150 rpm. After the desired amount of organic dye in 50 mL of the aqueous solution was added into the reactor, the reaction was initialized by adding OMS-2 and PMS. Since PMS is an acidic oxidant, the addition of PMS led to a significant decrease of pH, and the experiment was conducted at acidic medium (pH 3.84, no adjustment). For studying the effect of solution pH on the rate of Acid Orange 7 (AO7) degradation, H_2SO_4 (20 mM) and NaOH (20 mM) was used to adjust the solution pH after PMS was added into the solution. For the recycling experiment, the catalyst was separated without any treatment after each recycle, and then the next reaction was started by adding a fresh solution of AO7 and PMS.

2.4. Analysis

To monitor the degradation process of organic dyes, solution samples were taken out at given time intervals with solid removal and measured immediately on a Varian Cary 50 Scan UV–Vis spectrophotometer. All the measurements were conducted in triplicate with a mean deviation lower than 0.01 to ensure the reproducibility of experimental results. For the dyes AO7, Reactive Brilliant Blue KN-R (KN-R), Methylene Blue (MB), Rhodamine B (RhB), Reactive Brilliant Red X-3B (X-3B) and Methyl Orange (MO), their maximum absorption wavelengths are 484, 592, 664, 555, 538 and 464 nm, respectively. Initial rates of AO7 degradation were determined by the slope of kinetics curves at the beginning of reaction. The extinction coefficient of AO7 is 2.1 L/(mol cm), and its molar concentration was calculated by the Lambert–Beer's law. Total organic carbon (TOC) was determined by an Apollo 9000 TOC analyzer. The Mn ion leaching was monitored by atomic absorption spectroscopy (AAS, Analyst 300, P.E. Inc.).

For identification of degradation products, the samples were analyzed by mass spectrometry, and the experiments were performed on an Esquire LC–ion trap mass spectrometer (Bruker Daltonics, Bremen, Germany) equipped with an orthogonal geometry ESI source. Nitrogen was used as the drying (3 L/min) and nebulizing (6 psi) gas at 300 °C. The spray shield was set to 4.0 kV and the capillary cap was set to 4.5 kV. Scanning was performed from m/z 70 to 800 in the standard resolution mode at a scan rate of 13 kDa/s. Before analysis, each sample was diluted ten times.

3. Results and discussion

3.1. Characterization of OMS-2

The X-ray diffraction patterns of OMS-2 catalysts prepared by a reflux method are shown in Fig. 1(A). All peaks can be indexed to pure cryptomelane phase (JCPDS 29-1020) and no other phases are present. The peaks for OMS-2 are weak and broad, indicating the crystallite size is small. By using the Scherrer equation for the (2 1 1) peak from XRD data, the value was calculated to be 11 nm, which was slightly smaller than that made by reflux, but larger than that prepared by solvent-free method in literature [29]. Fig. 1(B) displays the FT-IR spectra of OMS-2. The bands at around 3430 and 1630 cm^{-1} are due to the stretching and bending vibration of hydroxyl groups. The peaks at about 717, 531 and 478 cm^{-1} can be attributed to the vibrations of the MnO_6 octahedral framework, which are the characteristic peaks of cryptomelane [32].

To examine the surface area, as well as the pore size distribution, nitrogen adsorption/desorption analysis was conducted on OMS-2. N_2 sorption isotherms are shown in Fig. 2. Typical Type II adsorption

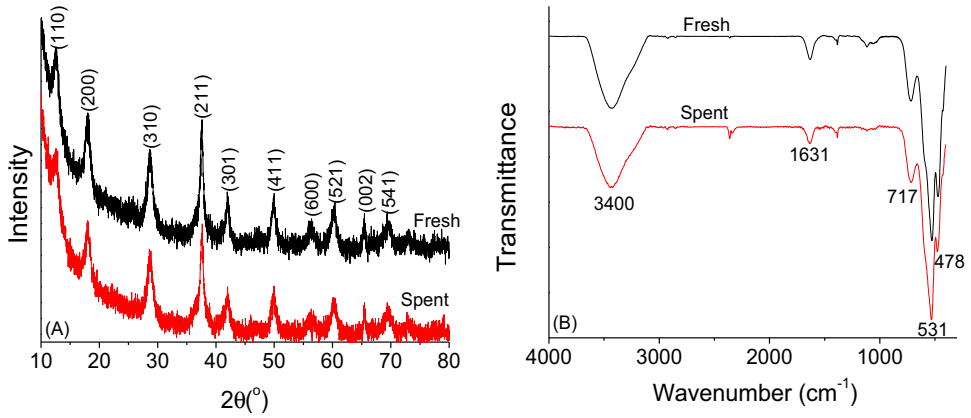

Fig. 1. (A) XRD and (B) FT-IR spectra of fresh and used OMS-2 catalyst.

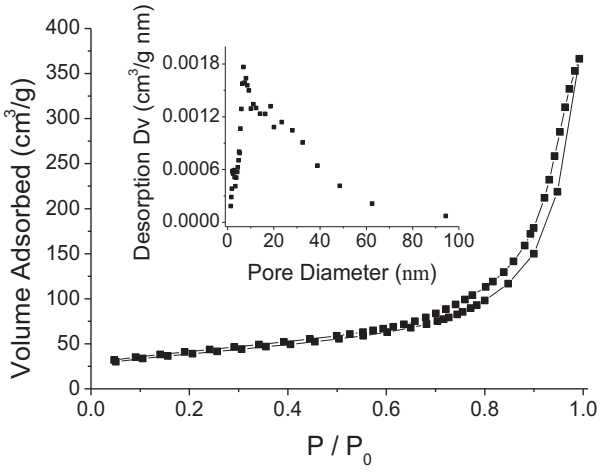

Fig. 2. N_2 adsorption/desorption isotherm curve of the synthesized OMS-2 catalyst. Inset is the pore size distribution of OMS-2.

isotherms were observed. The inset of Fig. 2 shows a mesopore size distribution calculated by the Barrett–Joyner–Halenda method. As can be seen, a narrow pore size distribution in the range of 2–50 nm for the catalyst was observed with a major peak centered at 7 nm. A large total pore volume of 0.57 cm^3/g and an average pore size of about 17.1 nm were also observed. The mesopore volume was 0.46 cm^3/g, constituting about 81% of the total pore volume of the sample. The measurement of Brunauer–Emmet–Teller (BET) surface showed that the synthesized catalyst had a BET surface area of 133 m^2/g, a little higher than that for the reported OMS-2 catalyst with the similar preparation method [29,33]. The contribution of the mesopores to the total BET surface area was also up to 81%.

The morphology of OMS-2 is shown in Fig. 3. Based on the SEM images, the catalyst has a fine and uniform nanofiber shape. The range of diameters of these nanofibers is about 10–20 nm and the range of lengths is about 100–500 nm. The size is much smaller than that of the material fully made by the method reported in the literature [33]. As can be seen in Fig. S1, the nanofibers synthesized are about 20–40 nm in diameter, and greater than 400 nm in length. This may be caused by the different mixing temperature of Mn salts. In literature, the solution of $MnSO_4$ was mixed with $KMnO_4$ solution at room temperature [33], while in our experiments $KMnO_4$ was added into the $MnSO_4$ solution at the reflux temperature. However, a more detailed understanding of the mechanism needs to be studied further.

3.2. Catalytic activity of OMS-2

The catalytic performance of different catalysts is shown in Fig. 4. From Fig. 4(A) it can be seen that OMS-2 showed high efficiency for AO7 degradation with a removal of 93% after 10 min in the presence of PMS, while the addition of PMS in the absence of the catalyst brought about only 2.3% of AO7 removal. For the experiment with only OMS-2, the removal of AO7 was 41% within the same time, probably due to the adsorption of AO7 on the surface of the catalyst. The high efficiency of OMS-2 could be further

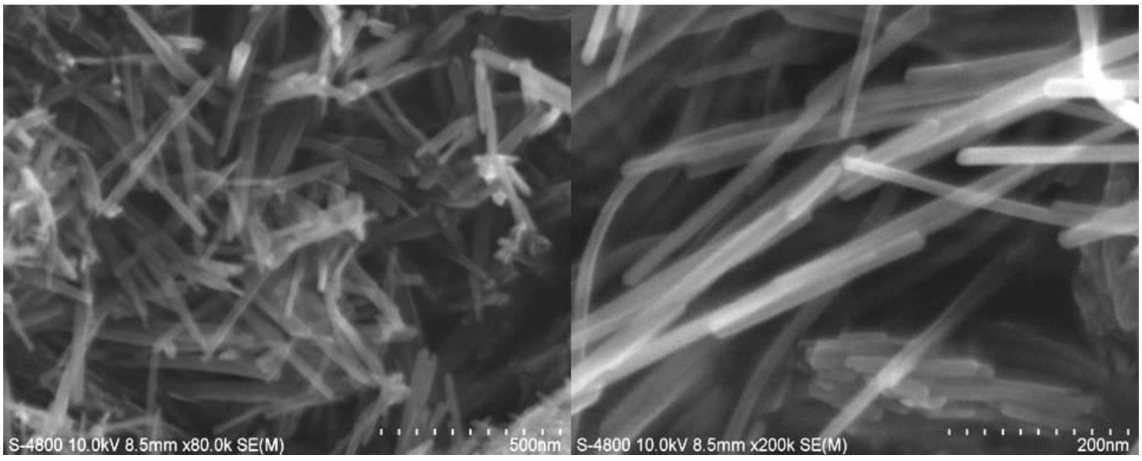

Fig. 3. HRSEM images of OMS-2 catalyst.

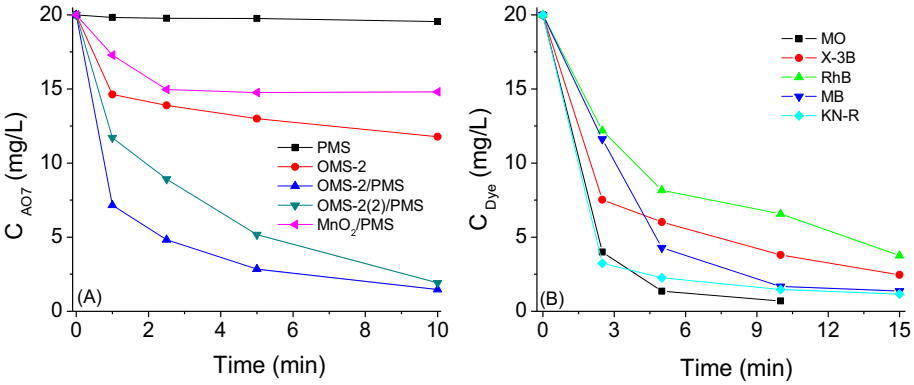

Fig. 4. (A) Degradation of AO7 with different systems and (B) degradation of other organic dyes with OMS-2/PMS system. Conditions: OMS-2 0.25 g/L, MnO_2 0.25 g/L, PMS 0.25 g/L, Dye 20 mg/L, 25 °C.

confirmed by the experiment carried out under a high concentration of AO7 (200 mg/L) or a low concentration of the catalyst (0.0625 g/L), as described in Figs. 6 and 7 in Section 3.3. The OMS-2 (2) catalyst showed a slightly slower degradation rate in comparison with OMS-2, probably due to it's greater sizes. In the past few years, several Mn-based catalysts such as MnO, Mn_2O_3, Mn_3O_4 and MnO_2, have been found to be active in PMS decomposition for aqueous organic pollutants oxidation [25]. Here, α-MnO_2 has also been prepared according the method described in literature [23] and tested as the catalyst for AO7 degradation. However, its activity was very slow with only a removal of 28% in 10 min. The superior catalytic activity of OMS-2 may be ascribed to coexistence of mixed-valent manganese species Mn(IV) and Mn(III) as active site on the catalyst surface. In addition, the activity of the OMS-2/PMS system for degradations of other organic dyes with different

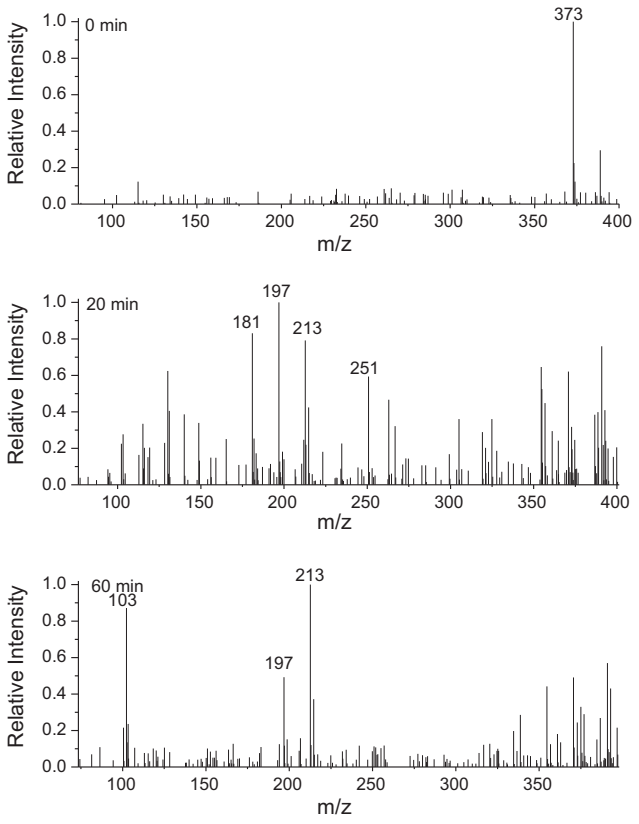

Fig. 5. ESI(+) mass spectra of AO7 solution during degradation with OMS-2/PMS system. Conditions: AO7 100 mg/L, PMS 0.6 g/L, OMS-2 0.25 g/L, 25 °C.

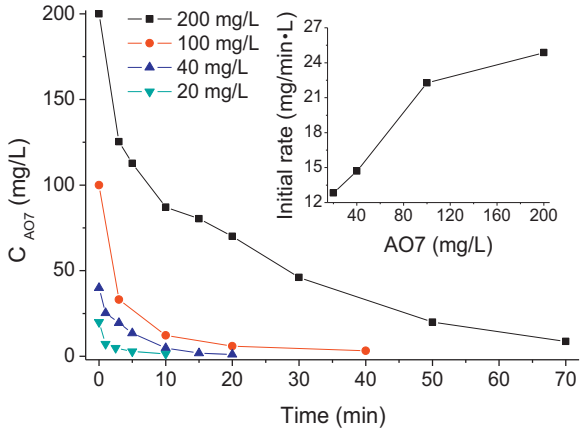

Fig. 6. Influence of AO7 concentration on AO7 degradation. Inset: A plot of initial degradation rate versus AO7 concentration. Conditions: OMS-2 0.25 g/L, PMS 0.25 g/L, 25 °C.

chemical structures such as the anthraquinone dye KN-R, the quinone imine dye MB, the xanthene dye RhB, the azo dye X-3B and MO was examined under similar conditions. As shown in Fig. 4(B), all the pollutants could also be decomposed efficiently. These results clearly indicated that the OMS-2/PMS is an efficient catalytic system for remediation of dyes wastewater.

To further ascertain the efficiency of OMS-2/PMS system for AO7 degradation, UV–Vis spectra and ESI–MS were used to identify

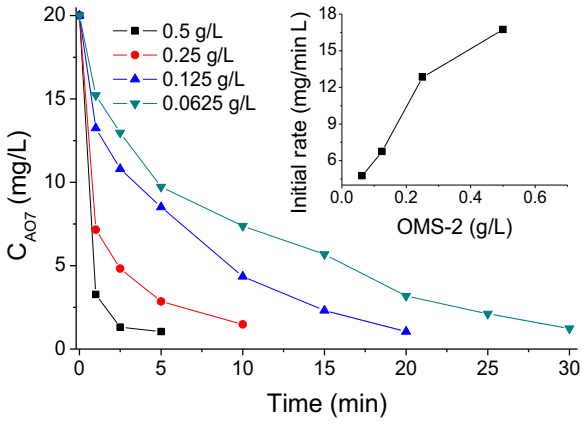

Fig. 7. Influence of OMS-2 concentration on AO7 degradation. Inset: A plot of initial degradation rate versus OMS-2 concentration. Conditions: PMS 0.25 g/L, AO7 20 mg/L, 25 °C.

the degradation products. Representative UV–Vis spectra changes observed during reaction are depicted in Fig. S2. For AO7 solution before reaction, it shows a main absorption bands at 484 nm, corresponding to the n–π* transition of the azo form, and another two bands at 230 and 310 nm in ultraviolet region, which is attributed to the π–π* transition of the benzoic and naphthalene ring, respectively [34]. Addition of PMS into the aqueous solution caused the absorption bands of the dye in the visible region to decrease with time and finally to disappear, indicating the destruction of its chromophoric structure in the vicinity of the azo-linkage. At the same time, the decrease of the two bands in ultraviolet region was observed, due to the opening of the benzene and naphthalene ring. In addition, the absorbance at 254 nm first increased at the first 2.5 min and then descended gradually in the late reaction stage (inset of Fig. S2). The change can be attributed to the formation and degradation of anaphthalene type intermediates [34]. Although AO7 was completely destructed within 20 min at 100 mg/L AO7, 0.25 g/L OMS-2 and 0.60 g/L PMS, only 8% TOC removal was obtained after 18 h. This was probably caused by the low dosage of PMS, as a complete mineralization of 100 mg/L AO7 will consume 5.76 g/L PMS.

Fig. 5 shows the change of ESI–MS spectra of AO7 solution at positive ion mode during reaction. At the beginning of the reaction, an intense ion of *m/z* 373 corresponding to $[AO7+Na]^+$ was observed as expected. After 20 min treatment, the intensity of AO7 at *m/z* 373 decreased significantly, indicating that it was degraded into some intermediate products. Meanwhile, the peaks at *m/z* 181, 197, 213 and 251 showed up. They could be attributed to 1,2-naphthaquinone and its further oxidized compounds. According to the literature, the toxicity of naphthaquinone from AO7 degradation is even higher than that of the azo dye [35], fortunately, the compound can be easily degraded by the system. After 60 min, the peaks attributed to naphthaquinone at *m/z* 181 completely disappeared with another new peak at *m/z* 103 appeared.

Based on above analysis, a schematic degradation pathway of AO7 by the OMS-2/PMS system was proposed and is given in Fig. S3. During oxidation, AO7 was attacked by the active species, especially $SO_4^{-\bullet}$, and then decomposed to and 1,2-naphthaquinone and *p*-phenolsulfonic acid, detected by ESI–MS at negative ion mode. Afterward, the 1,2-naphthaquinone was further attracted by the radicals to hydroxylated or polyhydroxylated derivatives, and finally to carboxylic acids by ring opening.

3.3. Effect of several parameters on catalytic activity of OMS-2

The practical application of the catalyst requires a preliminary evaluation of the effect of various operation parameters on their catalytic performance. For that reason, the effect of major factors including AO7 concentration, OMS-2 concentration, PMS concentration, and pH, on the catalytic behavior of OMS-2 was studied. The influence of initial AO7 concentrations at 20, 40, 100 and 200 mg/L on the degradation efficiency is presented in Fig. 6. From the inset, it can be seen that the degradation efficiency enhanced with the increasing of AO7 concentration, as the initial rate of AO7 removed increased from 12.8 to 24.9 mg/min L. However, the initial rate did not increased linearly at the high AO7 concentration of 200 mg/L, probably owing to the fact that the high amount of adsorbed dye molecules on the catalyst at a high concentration of AO7 hindered the reaction between OMS-2 and PMS. Besides, increased with AO7 concentration, the amount of dye in solution will require more time to achieve a complete removal, due to the same concentrations of produced reactive radicals under the same concentrations of OMS-2 and PMS. For example, at a concentration of 20 mg/L, the complete AO7 removal was achieved in about 5 min, while at concentrations of 40, 100 and 200 mg/L, the time needed for complete removal of the dye was 20, 40 and 70 min, respectively.

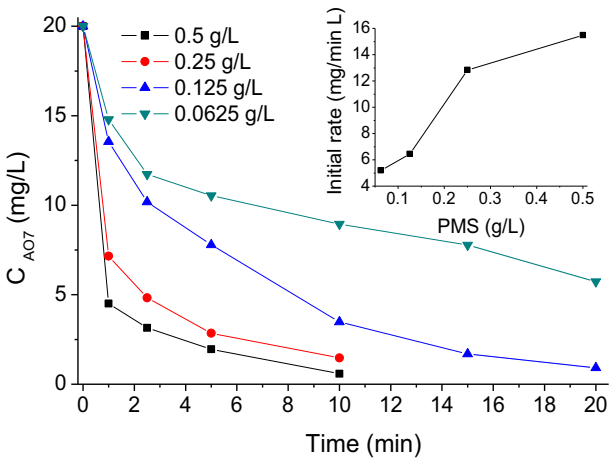

Fig. 8. Influence of PMS concentration on AO7 degradation. Inset: A plot of initial degradation rate versus PMS concentration. Conditions: OMS-2 0.25 g/L, AO7 20 mg/L, 25 °C.

Fig. 7 illustrates the change of AO7 concentration with time at different catalyst dosages in solution. As expected, an enhancement of AO7 degradation was observed by increasing OMS-2 concentration from 0.0625 to 0.5 g/L. A 94% removal of AO7 was reached within 30 min at 0.0626 g/L OMS-2. While the same removal could be reached within 20, 10 and 5 min at OMS-2 loading of 0.125, 0.25, and 0.50 g/L, respectively. The fact is evidently attributed to the increased concentration of active sites for reaction with PMS, which will generate more reactive radicals. In addition, the dye adsorbed on the catalyst increased with OMS-2 dosage, which could also enhance the degradation rate. At a concentration of 0.0625 g/L, the amount of the dye adsorbed onto the catalyst was about 13% after 10 min in the absence of PMS; but under a concentration of 0.5 g/L, about 60% of the dye was removed by adsorption within the same time. However, the efficiency did not increase linearly at the high concentration of OMS-2. Perhaps under the conditions the diffusion of AO7 and PMS was the rate-limiting step.

In what concerns the treatment process efficiency and operational costs, PMS has a high impact. To elucidate the role of PMS concentration on the degradation of AO7, some experiments were carried out by varying the initial PMS concentrations. As shown in Fig. 8, AO7 was slowly degraded in the presence of 0.0625 g/L PMS. Under the conditions, the molar ratio of PMS/AO7 was 4. The incomplete removal of AO7 was probably due to lack of sufficient oxidant amount. When PMS concentration increased to 0.25 g/L, the initial degradation rate increased (shown in the inset), as more active radicals could be produced under a high concentration of PMS. However, further increase in PMS concentration to 0.5 g/L did not result in the same increasing trend of the degradation efficiency. The fact may be due to that the reaction proceeds via radical mechanism. The rate is limited by radical generation under low concentrations of PMS, but by radical attraction to the dye under a high PMS concentration.

The influence of initial solution pH on AO7 degradation was also studied at five different pH values of 2.65, 3.84, 6.68, 7.32 and 8.41, respectively. The results in Fig. 9 demonstrated that the degradation rate decreased as pH rose from 2.65 to 8.41. In acidic medium, the dye could be nearly completely degraded within 10 min. At an initial pH of 7.32, the degradation rate became much slower; however, a removal of 93% could still be achieved within 60 min, implying that the catalyst still exhibited a good catalytic activity under neutral conditions. When the oxidation was carried out in alkaline medium (pH 8.41), a rapid degradation of AO7 during the first 5 min followed by a linear decreasing with a final removal of 66% after 60 min was observed. In the pH range of 2.65 to 8.41,

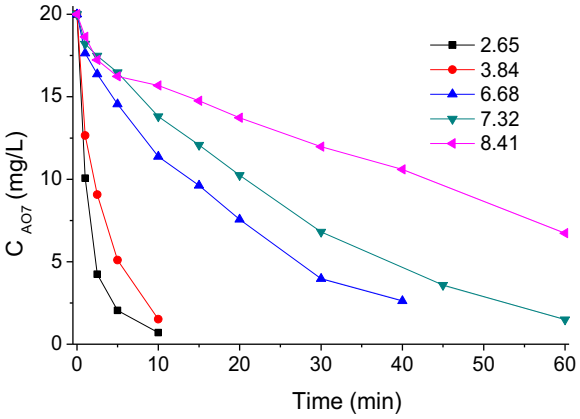

Fig. 9. Influence of pH on AO7 degradation. Conditions: OMS-2 0.25 g/L, PMS 0.25 g/L, AO7 20 mg/L, 25 °C.

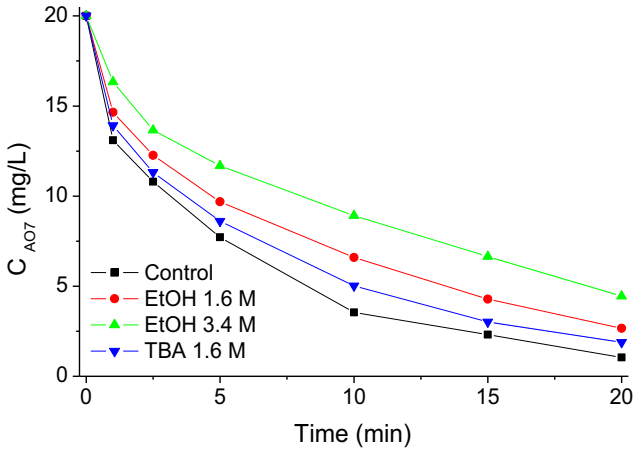

Fig. 11. Inhibiting effect of EtOH and TBA on AO7 degradation with the OMS-2/PMS system. Conditions: OMS-2 0.125 g/L, PMS 0.25 g/L, AO7 20 mg/L, 25 °C.

AO7 and PMS are presented as negative ions [36]; while increase of solution pH rise the amount of negative surface charge on the catalyst [37]. This possibly inhibits the static interactions between OMS-2 and AO7 or PMS, and consequently results in a slower rate of reactive species production and dye degradation. In addition, self-dissociation of PMS mainly through non-radical pathways increases with increase in solution pH, which would additionally reduce the degradation efficiency of target contaminant [38]. It is noted that the pH of solution reduced after reaction, due to the formation of acid intermediates.

3.4. Stability of OMS-2 catalyst

To test the stability and recyclability of OMS-2, the catalyst was collected by filtration after reaction, and the decolorization reaction was re-initiated by adding a fresh solution of AO7 and PMS. As shown in Fig. 10(A), the efficiency decreased during the second run in comparison with that in the first run, probably due to the reduction of adsorption ability. However, the catalyst was rather stable during the next runs, which could be used for five successive cycles with the removal of AO7 maintaining at about 91% after each run. During the first run, the Mn concentration in the reaction solution was found to be less than 0.1 mg/L by using AAS spectroscopy (Fig. 10(B)). Then another experiment was established to check whether the dissolved Mn ions were responsible for the observed catalytic activity. After the reaction, the catalyst was filtered and a fresh portion of AO7 and PMS was added to the filtrate with the same concentration as that before the catalytic test. In this case, no reaction proceeded. These results indicated that leaching of Mn into the liquid phase was negligible and the observed catalysis was intrinsically heterogeneous.

The separated OMS-2 catalyst after the fifth reaction run was further examined by using XRD and FT-IR with the results shown in Fig. 1. Compared with the images of the fresh catalyst, the XRD and FT-IR images of the recycled catalyst OMS-2 did not show any obvious structural changes. From FT-IR spectra, it could be also seen that no externally adsorbed species detected on the catalyst surface. At a higher pH value of 7.32, the catalyst was also stable during five successive cycles (Fig. S4). About 90% of AO7 was removed after each run. All these analyses indicated the excellent stability of OMS-2 catalyst.

3.5. Activation mechanism of PMS on OMS-2

Manganese oxides at different oxidation states can activate PMS to produce $SO_4^{-\bullet}$ and $SO_5^{-\bullet}$ [25]. HO• can be also generated by reaction of $SO_4^{-\bullet}$ with H_2O [21]. As the one-electron redox potential of $SO_5^{-\bullet}$ is estimated to be about 1.1 V at pH 7, which is much lower than that of $SO_4^{-\bullet}$ (2.43 V) and HO• (2.85 V), $SO_5^{-\bullet}$ is usually considered not responsible for the degradation of organic pollutants [21]. In order to understand the role of $SO_4^{-\bullet}$ and HO• radicals in the OMS-2/PMS system, alcohols including EtOH and TBA were added into the system as quenching agents. As shown in Fig. 11, in the presence of 1.6 M EtOH, the catalytic activity was slightly inhibited, and more addition of the alcohol (3.4 M) further decreased the rate

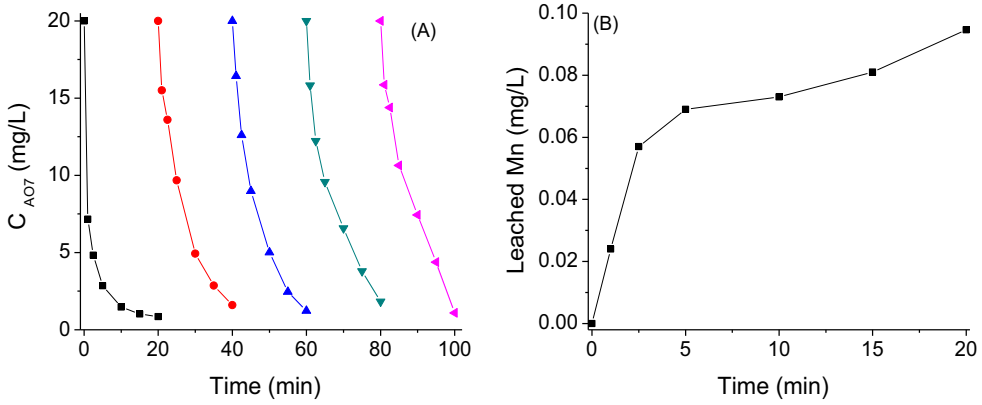

Fig. 10. (A) Degradation of AO7 using the recycled OMS-2 catalyst and (B) leaching of manganese from OMS-2 during the first run. Conditions: OMS-2 0.25 g/L, PMS 0.25 g/L, AO7 20 mg/L, 25 °C.

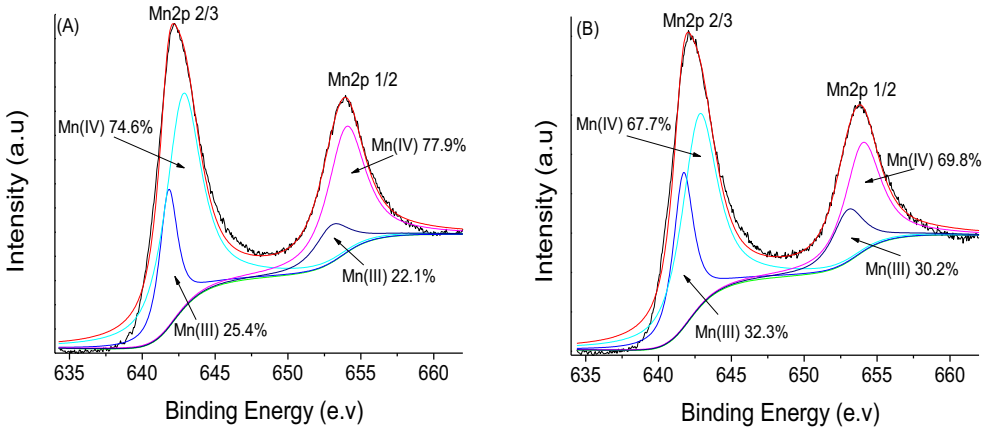

Fig. 12. High-resolution XPS spectra of the Mn 2p taken on the fresh (A) and used (B) OMS-2.

of AO7 degradation. In the presence of 1.6 M TBA, a much weaker inhibition effect was observed than that with the same molar concentration of EtOH. These results implied that $SO_4^{-\bullet}$ radicals were the main active species controlling the oxidation reaction in the OMS-2/PMS system. HO• radicals might also present, but its contribution was minor compared with $SO_4^{-\bullet}$ radicals.

In literature, the proposed activation process of PMS by manganese catalysts was similar to that by cobalt catalysts, which involves the generation of $SO_5^{-\bullet}$ radicals through the reduction of high-valent state of Mn species and the formation of $SO_5^{-\bullet}$ radicals by oxidation of the generated low-valent Mn species [25]. For example, MnO_2 and MnO may activate PMS via reduction and oxidation to generate $SO_5^{-\bullet}$ and $SO_4^{-\bullet}$, respectively, while Mn_2O_3 can produce $SO_5^{-\bullet}$ and $SO_4^{-\bullet}$ via disproportionation reaction [25]. Mn oxide based materials, notably OMS-2 are known to be effective and inexpensive oxidation catalysts due to their porosity, lattice oxygen availability, and coexistence of different valence states of Mn species, namely Mn(IV) and Mn(III) [29]. Therefore, we speculate that the highly catalytic activity of OMS-2 involved the activation of PMS meditated by the redox pair of Mn(IV)/Mn(III). To understand the roles of Mn species in the activation of PMS, the XPS spectra of OMS-2 were measured before and after the five degradation experiments. As shown in Fig. 12, the Mn 2p peak could be fitted well by a Gaussian–Lorentzian product function after Shirley type background subtraction. For Mn 2p 3/2, two peaks at 641.7 and 642.8 eV were obtained in the fresh OMS-2 catalyst (shown in Fig. 12(A)), which were assigned to Mn(III) and Mn(IV) oxidation states, respectively [39]. Their atom ratio was 25.4:74.6. After five successive reactions, the two Mn species were still present in the catalyst, but their atom ratio was changed to 32.3:67.7, indicating that Mn(IV) on surface of the used catalyst was transformed partially to Mn(III). From Mn 2p 1/2 shown in the figure, similar conclusions could be obtained.

The X-band ESR spectra of the OMS-2 catalyst are depicted in Fig. S5. For the fresh catalyst, only a peak around 3150 G was observed, which could be attributed to the Mn^{4+} ions [31]. Mn^{3+} species with d^4 configuration are difficult to monitor in X-band during ESR measurement because of the extreme spin–spin coupling of an even number electrons and very short relaxation time. In addition, the absence of the characteristic six-peak hyperfine structure for Mn^{2+} [31], implied that the divalent ions were not present in the prepared OMS-2 sample. After five successive reactions, the signal for Mn^{4+} species disappeared but without the appearance of Mn^{2+} ions suggested that Mn^{4+} was transformed to Mn^{3+} during the reaction. According to these analyses, the mechanism of activation of PMS by OMS-2 catalyst was proposed as follows:

$$\equiv Mn^{IV} + HSO_5^- \rightarrow \equiv Mn^{III} + SO_5^{-\bullet} + H^+ \quad (1)$$

$$\equiv Mn^{III} + HSO_5^- \rightarrow \equiv Mn^{IV} + SO_4^{-\bullet} + OH^- \quad (2)$$

$$SO_4^{-\bullet} + H_2O \rightarrow {}^{\bullet}OH + SO_4^{2-} + H^+ \quad (3)$$

4. Conclusions

OMS-2 was first used for oxidative degradation of organic dyes in aqueous solution through heterogeneous activation of PMS. Complete removal of AO7 and other dyes could be achieved within 15 min on the catalyst. Increasing the AO7 concentration, catalyst amount and PMS concentration promoted the dye degradation, while with the rise of solution pH, the efficiency decreased. OMS-2 also demonstrated stable performance in multiple runs. The quenching studies confirmed that sulfate radicals are the primary species produced during the catalytic decomposition of PMS. XPS and ESR results indicated that the catalytic mechanism might involve the reduction of Mn(IV) ions and the oxidation of Mn(III) ions by PMS. A schematic degradation pathway of AO7 by the OMS-2/PMS system was also proposed based on ESI–MS analysis. As a green oxidation process, the activation of PMS by OMS-2 may have potential application in wastewater treatment.

Acknowledgment

This work was supported by the National Natural Science Foundation of China (grant no. 21207105).

Appendix A. Supplementary data

Supplementary data associated with this article can be found, in the online version, at http://dx.doi.org/10.1016/j.apcatb.2014.09.008.

References

[1] X. Li, W. Shi, Q. Cheng, L. Huang, M. Wei, L. Cheng, Q. Zeng, A. Xu, Appl. Catal., A: Gen. 475 (2014) 297–304.
[2] A.D. Bokare, W. Choi, J. Hazard. Mater. 275 (2014) 121–135.
[3] P. Bansal, D. Singh, D. Sud, Sep. Purif. Technol. 72 (2010) 357–365.
[4] A. Hu, X. Li, Sh. Ye, G. Yin, Q. Zeng, Appl. Catal., B: Environ. 102 (2011) 37–43.
[5] A. Burg, I. Shusterman, H. Kornweitz, D. Meyerstein, Dalton Trans. 43 (2014) 9111–9115.
[6] G.P. Anipsitakis, D.D. Dionysiou, Environ. Sci. Technol. 38 (2004) 3705–4371.
[7] G. Fang, J. Gao, D.D. Dionysiou, C. Liu, D. Zhou, Environ. Sci. Technol. 47 (2013) 4605–4611.
[8] O.S. Furman, A.L. Teel, R.J. Watts, Environ. Sci. Technol. 44 (2010) 6423–6428.
[9] R.H. Waldemer, P.G. Tratnyek, R.L. Johnson, J.T. Nurmi, Environ. Sci. Technol. 41 (2007) 1010–1015.
[10] Q.J. Yang, H. Choi, D.D. Dionysiou, Appl. Catal., B: Environ. 74 (2007) 170–178.
[11] Q.J. Yang, H. Choi, S.R. Al-Abed, D.D. Dionysiou, Appl. Catal., B: Environ. 88 (2009) 462–469.
[12] F. Qi, W. Chu, B. Xu, Appl. Catal., B: Environ. 134–135 (2013) 324–332.

[13] J. Zhang, X. Shao, C. Shi, S. Yang, Chem. Eng. J. 232 (2013) 259–265.
[14] M. Stoyanova, I. Slavova, St. Christoskova, V. Ivanova, Appl. Catal., A: Gen. 476 (2014) 121–132.
[15] C. Tan, N. Gao, Y. Deng, J. Deng, S. Zhou, J. Li, X. Xin, J. Hazard. Mater. 276 (2014) 452–460.
[16] X. Chen, J. Chen, X. Qiao, D. Wang, X. Ca, Appl. Catal., B: Environ. 80 (2008) 116–121.
[17] W. Zhang, H.L. Tay, S.S. Lim, Y.S. Wang, Z.Y. Zhong, R. Xu, Appl. Catal., B: Environ. 95 (2010) 93–99.
[18] F. Ji, C. Li, L. Deng, Chem. Eng. J. 178 (2011) 239–243.
[19] F. Ji, C. Li, X. Wei, J. Yu, Chem. Eng. J. 231 (2013) 434–440.
[20] T. Zhang, H. Zhu, J.-P. Croue, Environ. Sci. Technol. 47 (2013) 2784–2791.
[21] Y. Ding, L. Zhu, N. Wang, H. Tang, Appl. Catal., B: Environ. 129 (2013) 153–162.
[22] Y. Guan, J. Ma, Y. Ren, Y. Liu, J. Xiao, L. Lin, C. Zhang, Water Res. 47 (2013) 5431–5438.
[23] E. Saputra, S. Muhammad, H. Sun, A. Patel, P. Shukla, Z. Zhu, S. Wang, Catal. Commun. 26 (2012) 144–148.
[24] H. Liang, H. Sun, A. Patel, P. Shukla, Z. Zhu, S. Wang, Appl. Catal., B: Environ. 127 (2012) 330–335.
[25] E. Saputra, S. Muhammad, H. Sun, H-M. Ang, M.O. Tadé, S. Wang, Appl. Catal., B: Environ. 142–143 (2013) 729–735.
[26] E. Saputra, S. Muhammad, H. Sun, H.M. Ang, M.O. Tade, S. Wang, Environ. Sci. Technol. 47 (2013) 5882–5887.
[27] E. Saputra, S. Muhammad, H. Sun, H-M. Ang, M.O. Tadé, S. Wang, Appl. Catal., B: Environ. 154–155 (2014) 246–251.
[28] Y. Yao, Y. Cai, F. Lu, F. Wei, X. Wang, S. Wang, J. Hazard. Mater. 270 (2014) 61–70.
[29] Y. Ding, X. Shen, S. Sithambaram, S. Gomez, R. Kumar, V.M.B. Crisostomo, S.L. Suib, M. Aindow, Chem. Mater. 17 (2005) 5382–5389.
[30] S.L. Suib, J. Mater. Chem. 18 (2008) 1623–1631.
[31] H.C. Genuino, Y. Meng, D.T. Horvath, C. Kuo, M.S. Seraji, A.M. Morey, R.L. Joesten, S.L. Suib, ChemCatChem 5 (2013) 2306–2317.
[32] L. Yu, M. Sun, J. Yu, Q. Yu, Z. Hao, C. Li, Chin. J. Catal. 29 (2008) 1127–1132.
[33] A. Iyer, H. Galindo, S. Sithambaram, C. King'ondu, C-H. Chen, S.L. Suib, Appl. Catal., A: Gen. 375 (2010) 295–302.
[34] M. Luo, L. Lv, G. Deng, W. Yao, Y. Ruan, X. Li, A. Xu, Appl. Catal., A: Gen. 469 (2014) 198–205.
[35] D. Mendez-Paz, F. Omil, J.M. Lema, Enzyme Microb. Technol. 36 (2005) 264–272.
[36] T. Zhang, H. Zhu, J.-P. Croué, Environ. Sci. Technol. 47 (2013) 2784–2791.
[37] M. Kosmulski, J. Colloid Interface Sci. 275 (2004) 214–224.
[38] A. Rastogi, S.R. Ai-Abed, D.D. Dionysiou, Appl. Catal., B: Environ. 85 (2009) 171–179.
[39] T. Zhang, X. Yan, D.D. Sun, J. Hazard. Mater. 243 (2012) 302–310.